

Feature Flow: In-network Feature Flow Estimation for Video Object Detection

Ruibing Jin, Guosheng Lin, Changyun Wen, Jianliang Wang, and Fayao Liu,

Abstract—Optical flow, which expresses pixel displacement, is widely used in many computer vision tasks to provide pixel-level motion information. However, with the remarkable progress of the convolutional neural network, recent state-of-the-art approaches are proposed to solve problems directly on feature-level. Since the displacement of feature vector is not consistent to the pixel displacement, a common approach is to: forward optical flow to a neural network and fine-tune this network on the task dataset. With this method, they expect the fine-tuned network to produce tensors encoding feature-level motion information. In this paper, we rethink this de facto paradigm and analyze its drawbacks in the video object detection task. To mitigate these issues, we propose a novel network (IFF-Net) with an In-network Feature Flow estimation module (IFF module) for video object detection. Without resorting pre-training on any additional dataset, our IFF module is able to directly produce feature flow which indicates the feature displacement. Our IFF module consists of a shallow module, which shares the features with the detection branches. This compact design enables our IFF-Net to accurately detect objects, while maintaining a fast inference speed. Furthermore, we propose a transformation residual loss (TRL) based on *self-supervision*, which further improves the performance of our IFF-Net. Our IFF-Net outperforms existing methods and sets a state-of-the-art performance on ImageNet VID.

Index Terms—Video Object Detection, Feature FLOW, Object Detection, Video Analysis, Deep Convolutional Neural Network (DCNN)

I. INTRODUCTION

OPTICAL flow, which indicates the pixel displacement is very popular in many computer vision tasks [1], [2], [3], [4], [5], [6], [7], [8]. People usually apply it to extract motion information. Recently, video object detection has witnessed rapid progress by using convolutional neural networks (CNN) [3], [4], [5]. These methods aim to leverage temporal information to enhance the feature representation at the current frame. Due to feature displacements existing across frames, they utilize optical flow (which expresses pixel displacement) generated by FlowNet [9] to estimate the feature displacement and align these feature maps according to the generated optical flow. After that, these aligned features are aggregated by weighted sum to produce an enhanced feature map for detection. Although good performances are achieved by these methods, these methods are limited by three drawbacks as discussed below:

- Optical flow expresses pixel displacement in images. Since the feature displacement is not strictly consistent to pixel displacement, it is inaccurate to align features based on optical flow. The quality of aggregated features is degraded by this inaccurate alignment scheme (verified in Sec. IV-B), limiting the accuracy of detectors.

- As an external network, FlowNet [9] is used in these methods to generate optical flow. In these methods, they pre-train FlowNet on an additional dataset, Flying Chair [9] and then fine-tune it on the task dataset. This makes the training procedure complex. Additionally, FlowNet, which consists of 23 layers, is computationally expensive and occupies large GPU memory. This also limits the number of aggregated frames during training and testing. Overall, these optical flow based methods are inefficient in training and inference.
- Domain gap exists between optical flow training datasets and the target task datasets. Trained in an external optical flow dataset, FlowNet cannot adapt well to the video object detection task (discussed in Sec. IV-B). This further degenerates the aggregated features and affects the accuracy of detectors.

These FlowNet based methods [3], [4], [5] propose the temporal aggregation part following a well-established paradigm: pre-train on an additional dataset and fine-tune the trained model on the task dataset. However, after analyzing their drawbacks, we question this paradigm and explore a brand new method without the pre-training process.

In this paper, we propose a novel neural network, which is able to directly predict **feature flow**, indicating the feature displacement. An In-network Feature Flow estimation module (IFF module) is proposed in this network and our proposed method is called IFF-Net. Different from FlowNet based methods, the IFF module does not require the pre-training process.

Benefited from the feature flow generated by our IFF module, our IFF-Net could align and aggregate features better than optical flow based methods. It provides a solid foundation for accuracy improvement of detectors.

Additionally, our IFF module shares the network backbone with detection branches, which prevents IFF-Net from the overhead computation in FlowNet and makes feature flow estimation nearly cost-free. Without resorting to any additional neural network, our IFF-Net could aggregate temporal feature and predict results in a **single** network. Furthermore, our IFF module does not need any additional dataset for training. So, our IFF-Net is effective and efficient in both training and inference.

IFF-Net is trained in an end-to-end manner, which makes the feature flow generated by our IFF module adapt well to this task. This helps to improve the quality of aligned features further. In contrast to optical flow based methods, we do not have the issue of domain gap due to networks training in additional optical flow datasets.

Since features highly depend on trained models, it is difficult to do annotations for feature flow in training datasets. Instead of fully supervised training, we propose the transformation residual loss (TRL) to improve the performance of IFF module in *self-supervised* learning. It is used as an additional loss in *training*. After employing TRL, feature flow from our IFF module is improved with negligibly additional computation cost. The performance of IFF-Net is also improved.

Our contributions can be summarized as follows:

- 1) We propose a novel network (IFF-Net) with an in-network feature flow estimation module (IFF module). Compared with optical flow, our IFF module does not require the pre-training progress. Without the needing of additional training datasets, the domain gap problem in optical flow based methods is avoided. Additionally, feature flow produced by our IFF module is better at feature alignment than optical flow. By sharing features with detection branches, the feature flow estimated by our IFF module is nearly cost-free, enabling efficient feature aggregation. Our IFF-Net is efficient in training and inference.
- 2) IFF-Net is trained in an end-to-end manner. A transformation residual loss (TRL) is also introduced as a self-supervision method, which improves our IFF module further and boosts up the performance of IFF-Net.
- 3) Seq-NMS [10] is widely used in many approaches for video object detection as a post-processing method. We improve Seq-NMS (denoted as Seq-NMS+) and apply this modified version to further boost the performance of our IFF-Net
- 4) We have carried out extensive experiments to verify the effectiveness of our method. IFF-Net outperforms all existing methods and achieves a new state-of-the-art accuracy on the ImageNet VID [11] while maintaining a fast inference speed.

II. RELATED WORK

Object detection in static images. Object detection methods for static images are proposed to utilize the appearance information from images to accurately detect objects. Currently, state-of-the-arts methods [12], [13], [14], [15], [16], [17], [18], [19], [20], [21], [22] are mainly based on neural networks and the deep learning technology.

These methods fall into two categories: two-stage and one-stage methods. Two-stage methods decompose object detection into two stages: proposal generation and object detection. Two-stage methods firstly utilize some algorithms to produce the proposals, which may include objects. After that, they apply a detector on these proposals to detect objects.

Among two-stage methods, R-CNN is firstly proposed in [12], where a CNN based method is proposed to classify each proposal region for object detection. However, this method is time-consuming and requires much disk space. To improve the training and testing speed, a ROI Pooling layer [13] is proposed in Fast R-CNN [13]. In Fast R-CNN, the feature map for the whole image is shared during proposal classification. By using computation sharing, the training and testing speed is

improved. Then, the Region Proposal Network (RPN) in Faster R-CNN [14] is proposed by sharing the feature map of Fast R-CNN. Benefiting from the end-to-end training, Faster R-CNN shows a faster speed while remaining a better detection accuracy. Following Faster R-CNN, many detection approaches [15], [16], [17] are proposed for better performance.

For one-stage methods, they detect objects only in one-step. These approaches are able to detect objects in a fast speed, while sacrificing the detection accuracy. Among deep learning based methods, OverFeat [18] is firstly proposed to use feature map from CNN to detect objects in a sliding window manner.

After that, YOLO [19] and SSD [21] are proposed for further improving one-stage detection methods. YOLO is short for *You Only Look Once*, which is able to detect objects in a extremely fast speed, 155 fps. It unifies the detection framework into a single neural network. In YOLO, a full image is divided into a grid of sub-regions and detection results for each sub-region are predicted. Single Short multibox Detector (SSD) proposes a multi-scale feature based detection framework. Compared with YOLO, SSD progressively generates feature maps in different resolutions and applies its detector on each feature map to provide final results. These two detection methods show better results on PASCAL [23] than OverFeat. After that, RetinaNet [22] proposes a focal loss for improving the detection accuracy in one-stage methods and yields comparable performance to two-stage detectors.

Object detection in video. Different from static image based object detection, video object detection aims to utilize temporal information for performance improvement. They can be roughly divided into two types: box-level and feature-level methods. In the box level methods, they leverage temporal information on box-level [10], [24], [25]. The bounding boxes, which are predicted in each frame, are linked along the temporal dimension as a sequence. These linked boxes are then re-scored according to the distribution of the original scores.

Compare with box-level methods, many approaches [26], [3], [4], [27], [28], [29], [30], [31], [32] are proposed to aggregate temporal information in feature level. For the feature aggregation methods, they can be roughly divided into two categories: proposal-level and whole feature map level feature aggregation. In the proposal-level aggregation, methods in [33], [26], [34] train a network to predict box offsets. Approaches in [31], [32] combine the features in the related proposals based on feature similarity. These methods store proposal features in each frame and fuse them in a post-processing methods. Without the limitation of the GPU memory, these methods are able to aggregate long-range temporal information. However, limited by the proposal regions, they cannot utilize the context region to improve the detection accuracy.

In comparison, many approaches [3], [4], [5], [29], [30] are proposed to aggregate the whole feature maps across frames and detect objects on these aggregated feature maps. Due to the displacement between two frames, they firstly align feature maps across frames and fuse these feature maps together. Some methods utilize optical flow, which is produced by FlowNet[9], to do feature alignment. However, optical flow is not consistent to the feature flow. Even though they finetune the FlowNet on the task dataset, their performances

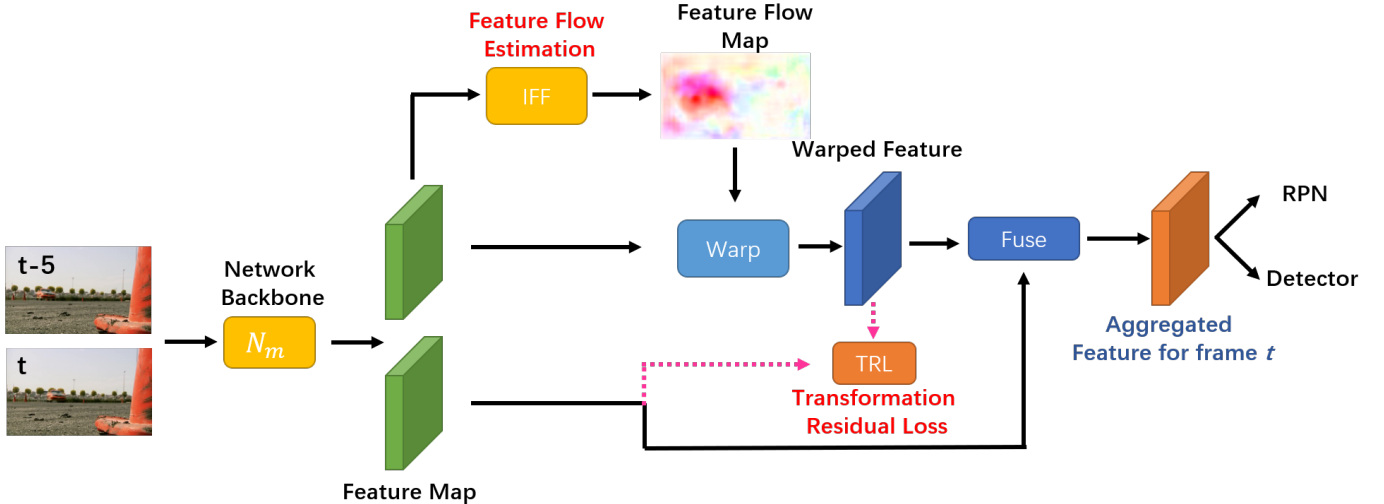


Fig. 1: The pipeline of IFF-Net (in-network feature flow estimation network) is illustrated in the case of fusing the features at the frame t with its neighboring features at the frame $t - 5$. The features at the frame $t - 5$ are warped to the features at the frame t via the FFM (feature flow maps) produced by our IFF module (feature flow estimation module). Then, aggregated features are generated by fusing the features at the frame t and the warped features at the frame $t - 5$. After that, the aggregated features are forwarded to RPN and a detector to produce results. The transformation residual loss (TRL) is applied only in the training process.

are not satisfactory. Additionally, FlowNet occupies much GPU memory, which causes that these methods can only aggregate nearby temporal information. This further degrades their performances. To alleviate these problems, some methods [27], [29], [28] try to explore temporal information on the whole feature map without FlowNet. Methods in [27], [29] aggregate features according to the feature vector similarity. STSN [28] directly uses deformable convolution layers to aggregate features across frames. Motion estimation and feature alignment across frames are not explicitly involved in STSN. The temporal aggregation module in them are too simple and cannot aggregate the temporal features accurately. Limited by this issue, their performances are not promising.

To alleviate these drawbacks of the methods discussed above, we propose IFF-Net, which directly predicts feature flow and enable us to align feature map in a more accurate way. Our IFF module shares the network backbone with detection branches. This prevents our IFF-Net from the overhead computation in FlowNet and enable our IFF module to leverage long-range temporal information. IFF-Net does not need any external dataset for training. Compared to other methods, our IFF-Net achieves better performance, though we use a smaller network and require fewer training datasets.

III. MAIN WORK

Our proposed network, IFF-Net is composed of a network backbone N_m and three branches (in-network feature flow estimation module, detector network and region proposal network), with the overall network shown in Figure 1. Given L preceding frames of a video, i.e. I_t , $t = 1, \dots, L$, N_m produces feature maps F_t for each of them. The number of aggregated features from neighboring frames are denoted as

τ . For convenience, we discuss our framework in the case of $\tau = 1$ in the following parts, as it is similar for other values of τ . IFF module produces the corresponding feature flow map (FFM), $M_{j \rightarrow i}$, for features from a pair of images I_i and I_j , where I_i is the image at the current frame and I_j is the image at its neighboring frame. Inspired by FGFA [3], the feature map from I_j is then warped to I_i based on the $M_{j \rightarrow i}$. The warped feature map $F_{j \rightarrow i}$ is obtained as:

$$F_{j \rightarrow i} = \mathcal{T}(F_j, M_{j \rightarrow i}), \quad (1)$$

where \mathcal{T} is a bilinear warping function. After that, feature aggregation is performed via a weighted sum operation on features at the current frame and other warped features according to FGFA. The aggregated feature is then passed to RPN and a detector to make predictions. As an additional loss, the TRL is used for self-supervised learning in the training process. Our IFF-Net is a single network and can be trained end-to-end.

A. In-network Feature Flow Estimation Module

In this section, we present the in-network feature flow estimation module (IFF module) to produce **feature flow** for feature alignment across frames. Our IFF module is built in IFF-Net itself and shares network backbone with detection branches.

Given two feature maps F_i and F_j , our IFF module predicts a feature flow map (FFM), which expresses feature flow. Two kinds of IFF modules are introduced in this part, as illustrated in Figure. 2 and Figure. 3, respectively.

Basic IFF Module. Basic IFF module is illustrated in the Figure 2, which is a basic version of our IFF module. It consists of three convolutional layers and a concatenation layer. A feature map of the current frame F_i and a feature

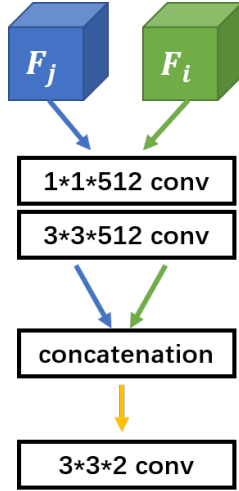


Fig. 2: Basic structure for feature flow estimation module (IFF module). F_i denotes the feature of the current frame and F_j denotes the feature of its neighboring frame.

map of its neighboring frame F_j are fed into the first two convolutional layers ($1 \times 1 \times 512$ kernels and $3 \times 3 \times 512$ kernels), separately. After that, these two produced features are concatenated together and forwarded to a convolutional layer ($3 \times 3 \times 2$ kernels) which predicts the corresponding FFM.

Benefiting from end-to-end training, our proposed IFF-Net with basic IFF module performs comparably to optical flow based methods like FGFA. FlowNet used in FGFA is composed of 23 layers, whereas our basic IFF module only consists of 4 layers. This shows that our basic IFF module is able to align features across frames in a more accurate and faster way than FlowNet. To further improve our IFF module performance, we propose an advanced version as follows.

Advanced IFF Module. To improve the performance of our IFF module, an advanced IFF module is proposed in this part. The spatial relationship between the current frame and its neighboring frame may provide important information for feature flow estimation. Inspired by it, we explicitly produce this relation information and fuse it with the feature map of the current frame (which undergoes an element-wise addition merger) in the advanced IFF module. The structure of this advanced IFF module is illustrated in the Figure 3.

Inspired by ResNet [35], the first two layers in the basic IFF module is replaced by a residual block, which is called embedded block 1 abbreviated as EB-1. Its structure is shown in Figure 4 (a). It consists of three convolutional layers with $1 \times 1 \times 512$ kernels, $1 \times 1 \times 512$ kernels, and $3 \times 3 \times 512$ kernels.

After that, the two features are concatenated together and passed to a correlation layer [9] to produce the relation information between two features. The correlation layer is defined as:

$$o(x, y) = \frac{\mathbf{F}_i(x, y) \cdot \mathbf{F}_j(x + d_x, y + d_y)}{c}, \quad (2)$$

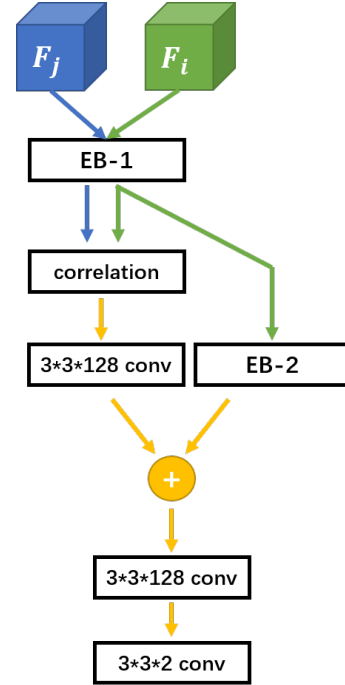


Fig. 3: Advanced structure for feature flow estimation module (IFF module).

where $\mathbf{F}_i(x, y)$ and $\mathbf{F}_j(x + d_x, y + d_y)$ are two feature vectors at (x, y) and $(x + d_x, y + d_y)$, respectively. c is the channel number in this feature map and $\mathbf{d} = (d_x, d_y)$ denotes the offset between two feature vectors, $F_i(x, y)$ and $F_j(x + d_x, y + d_y)$. Correlation is operated in a square neighborhood $D \times D$ in pixel with $D = 2\bar{d} + 1$, where \bar{d} is the maximum displacement. A stride s is used in F_j to sample on the feature map F_j . So, the size of correlation feature map is $w \times h \times (2 \times \bar{d}/s + 1)^2$, where w and h are the width and height of the feature map F_i or F_j .

To perform element-wise addition merger, the relation information and the feature map of the current frame are converted into a 128-dimension feature map. The result of the correlation layer is passed to a convolutional layer ($3 \times 3 \times 128$ kernels). The features of the current frame produced by EB-1 are passed to another embedded block denoted as EB-2, which is illustrated in Figure 4 (b). EB-2 is similar to EB-1. The difference is that the channel of kernels for layers in EB-2 are changed to 128. After merging, the fused feature map is passed to two convolutional layers ($3 \times 3 \times 128$ kernels and $3 \times 3 \times 2$ kernels) to produce a FFM.

After applying our advanced IFF module to IFF-Net, a better performance is achieved. Compared with FlowNet based methods [3], [5], our IFF-Net with this advanced IFF module is significantly better, though this advanced IFF module only consists of 9 layers, much smaller than FlowNet (23 layers). To further improve the performance of our IFF-Net, we develop a Transformation Residual Loss (TRL) and present it in the next part.

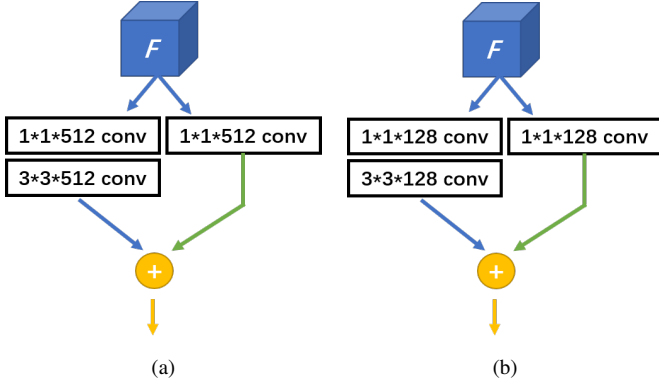


Fig. 4: Illustration of the structure of EB-1, shown in (a), and EB-2, shown in (b).

B. Transformation Residual Loss

Since features are highly related to trained models, it is difficult to do annotations for feature flow in training datasets. To further improve IFF module performance, we develop a transformation residual loss (TRL) in a self-supervised learning. We adapt the main formulation in TV-L1 [36] into our framework. It is used as an additional loss to our IFF module in the training process. This modified formulation (TRL) is written as follows:

$$\mathbf{L}_{TRL} = \lambda \frac{1}{N_p * d} \sum_{\mathbf{p} \in \Omega} \text{smoothL}_1[\Phi(F_j(\mathbf{p})) - F_i(\mathbf{p})], \quad (3)$$

where \mathbf{p} denotes a location on a feature map F , Ω denotes all locations of a feature map, N_p denotes the number of feature vectors in a feature map and d represents the number of channels for a feature vector. A trade-off weight λ is added. The transformation \mathcal{T} in Eq. (1) is used as $\Phi(\cdot)$ in Eq. (3). As this additional loss involves a transformation, we refer to it as transformation residual loss (TRL).

The temporal consistence between warped feature maps and the feature map from the current frame is involved explicitly in TRL. When training with TRL, the performance of IFF-Net is improved, surpassing methods [3], [5].

C. Modified Seq-NMS

Seq-NMS [10] has shown effectiveness in approaches [3], [27]. It proposes a post-processing method, which produces sequences along the temporal dimension in three steps: sequence selection, sequence re-scoring and suppression.

In this paper, we make two major modifications. Firstly, the non-maximum suppression (NMS) originally applied at the third step is moved to the first step. Through experiments, we find that this modification improves the speed of Seq-NMS while does not sacrificing the detection accuracy.

Secondly, we jointly use average and max operation: $0.5 * \text{mean}(\cdot) + 0.5 * \text{max}(\cdot)$ at its second step. In the original Seq-NMS, only one operation (max or average) is applied at the second step. Average operation suppresses outliers along temporal dimension, while max operation enhances scores of linked boxes. In our modified version, we try to combine their

advantages together and modify the original operation at the second step. After employing our modifications, The performance of Seq-NMS is further improved. For convenience, this modified Seq-NMS is denoted as Seq-NMS+.

D. Network Architecture

The network structures in our proposed IFF-Net is presented as follows.

Network backbone. The ResNet-101 [35] pre-trained on the ImageNet classification dataset is used as our network backbone. To meet the requirement of our task, we modify it according to FGFA [3]. We remove the last average pooling layer and the fully connected layers. Also in the last block, we change the effective stride from 32 to 16, and set the dilation rate of the convolutional layers as 2. We also add a convolutional layer ($3 \times 3 \times 1024$ kernels) to the last layer and initialize it in random.

Detection network. R-FCN [15] is used as our detector network. We modify it according to the method in [5]. There are two branches, R-FCN sub-network and RPN sub-network. The first 512-dimension feature map is connected to RPN and the left 512-dimension feature map is passed to R-FCN. 9 anchors (3 scales and 3 aspects) are applied in RPN. RPN produces 300 proposals for each image. The groups in a position-sensitive score map is set as 7×7 . The 1024-dimension feature map of the last convolutional layer is fed into our IFF module.

IV. EXPERIMENTS

A. Experimental Setting

Datasets. Experiments are conducted on the ImageNet VID [11] dataset which is for video object detection. There are 3862 training videos and 555 validation videos with annotations of 30 classes. We train our model on a subset of ImageNet DET training set (only the same 30 classes as in ImageNet VID) and VID training set following the setting in previous methods [3], [33]. Following their protocols, training is performed on the training set and performance is evaluated on the validation set.

Motion Categories. Following the protocol of FGFA [3], we divide objects in ImageNet VID into three categories according to object motion speed. The object motion speed is measured based on the average of object ground truth intersection-over-unions (IOUs) across frames $[t - 10, t + 10]$. The objects with average IOU larger than 0.9 are classified into the slow category. For objects with average IOU $\in [0.7, 0.9]$, they belong to the middle category and the remaining objects are classified into the fast category. According to FGFA, the slow, middle and fast motion categories respectively occupy 37.9%, 35.9% and 26.2%.

Implementation details. SGD optimization is performed in the training process. 120K iterations are performed on 4 GPUs. Each GPU holds one image sampled from ImageNet DET or VID dataset. A learning rate of 10^{-3} is used for the first 71.25 K iterations, and a learning rate of 10^{-4} is set for the rest iterations. Images are resized to a shorter side of 600 pixels in both training and testing. Only two neighboring

TABLE I: Comparison between optical flow and feature flow in feature alignment. OptFlow-A and OptFlow-B apply optical flow to feature warping, while IFF-Net uses feature flow in feature alignment. This shows that optical flow is not suitable for feature alignment, while our feature flow is able to effectively align temporal features.

Method	mAP	mAP (slow)	mAP (middle)	mAP (fast)
baseline(R-FCN)	74.1	83.6	71.6	51.2
OptFlow-A	74.4	84.9	74.0	51.5
OptFlow-B	75.4	83.7	74.8	53.5
IFF-Net-B(ours)	76.4	85.3	75.0	54.6
IFF-Net-C(ours)	77.1	85.0	75.9	57.7

frames are warped during training. For the current frame t , two frames are sampled randomly in the range of $[t-10, t+10]$. λ in Eq. (3) is set as 0.65. In Eq. (2), the maximum displacement \bar{d} is 10 and the stride s is 2. In testing, the number of warped images is set as 20, which is the same as in FGFA.

B. Comparison between Optical FLOW and Feature Flow

Optical flow indicates pixel-level displacement across frames, which is not consistent to feature-level displacement. To show the limitation of optical flow in feature alignment, we firstly conduct five experiments listed in Table I and do comparison between optical flow and our proposed feature flow in feature alignment. Then, we illustrate some visualization results in the Figure. 5 and briefly discuss them.

Feature Alignment Experiments. In Table I, baseline(R-FCN) serves as our baseline, where we only apply R-FCN, an image based detection method, to each frame alone. There is no temporal information involved in baseline(R-FCN). In comparison, two experiments (denoted as OptFlow-A and OptFlow-B) are carried out by using FlowNet for temporal feature aggregation and R-FCN is applied to the aggregated feature. We also conduct two experiments, where we replace FlowNet with our proposed IFF module, which is denoted as IFF-Net-B and IFF-Net-C. All these five experiments are conducted under the same hyper-parameters.

In OptFlow-A, we use a FlowNet, which is **pre-trained** on the optical flow dataset, for feature alignment. To ensure feature alignment conducted with optical flow, we fix FlowNet and only fine-tune detection part in the task dataset. From the Table I, it can be seen that OptFlow-A performs similar to baseline(R-FCN) (74.4 v.s. 74.1). However, in OptFlow-B, we jointly fine-tune FlowNet and the detection parts during training. Compared with OptFlow-A, OptFlow-B shows 1 mAP improvement. *This shows that original optical flow is not suitable for feature alignment due to the difference between pixel-level displacement and feature-level displacement.*

To solve this problem, we replace the FlowNet in OptFlow-B with our proposed IFF module in IFF-Net-B and IFF-Net-C. IFF-Net-B uses our basic IFF module, and IFF-Net-C uses our advanced IFF module. From the Table I, although our basic IFF module only consists of three layers, it effectively improve the detection accuracy than OptFlow-B (76.4 v.s. 75.4). By employing our advanced IFF module in IFF-Net-C, the performance is further improved (77.1 v.s. 75.4).

In the experiment OptFlow-B, although we fine-tune FlowNet on the task dataset, the performance of FlowNet based method (75.4) is still inferior to our IFF-Net (76.4 and 77.1). *This shows that the domain gap between FlowNet training dataset and the task dataset hinders the performances of FlowNet based methods.*

According to this comparison between optical flow and our feature flow, it demonstrates that optical flow is not suitable for feature alignment. Our proposed IFF modules effectively solve this problem and show significant improvement.

Feature Flow Visualization and Discussion. To show our proposed feature flow clearly, we visualize some feature flow results and compare them with the corresponding optical flow in Figure. 5.

Original images are shown in the first column, while columns 2 to 4 respectively list their corresponding feature maps, the optical flows of FlowNet, and the FFM produced by our IFF module. These feature maps are accumulated along the channel axis. To show the effectiveness of our feature maps, we visualize the corresponding detection results on the last column. To show them more clearly, the regions of objects are zoomed in.

In the video detection task, we need to perform feature alignment for feature aggregation. As feature captures different information (semantics, context) from pixels, the estimated feature flow is different from optical flow (pixel displacement). Compared with optical flow, using feature flow is more suitable for performing warping in the feature level. Moreover, end-to-end training makes our estimated feature flow well adapted to our detection task, which leads to better performance than optical flow based methods.

C. Ablation Study

To show the effectiveness of our IFF-Net, the performance of baseline and our IFF-Net variants on ImageNet VID are listed in Table II.

Our baseline consists of ResNet-101 [35] and R-FCN [15] detector. It is a single-frame framework and the same as the baseline in the Table I. Its mAP is 74.1% on overall categories. In Table II, the mAP for fast motion category, 51.2%, is the lowest among three categories. This indicates that fast motion category is challenging. However, as the percentage (26.2%) of fast motion category in the validation set is the lowest in all categories, the mAP for all categories is still very high, that is 74.1%.

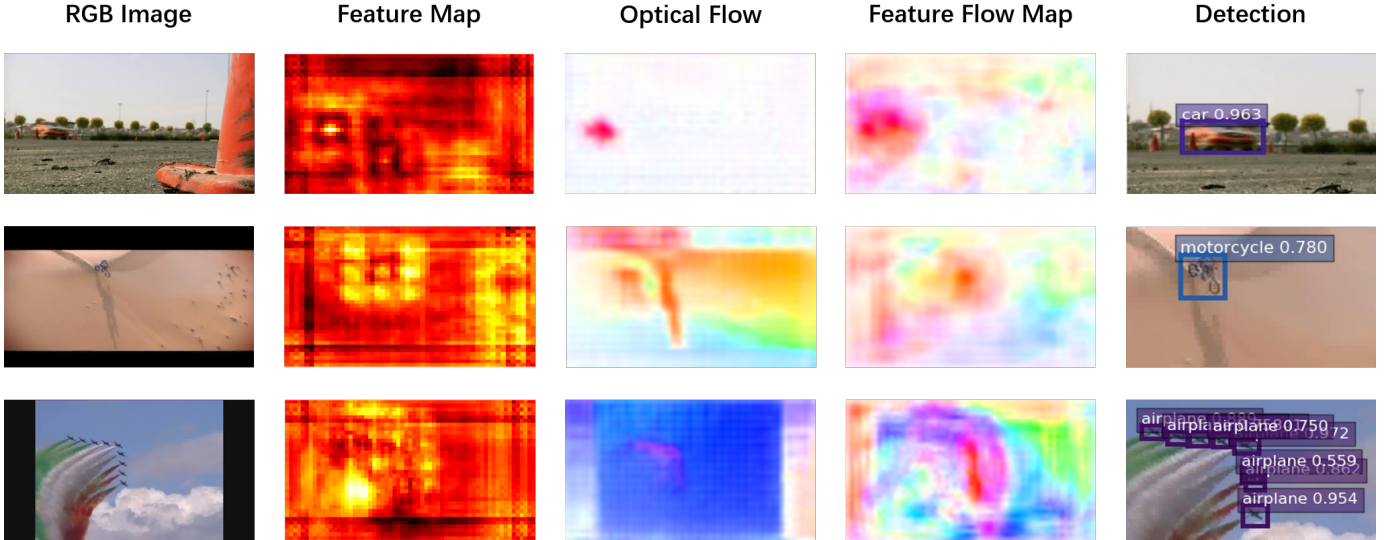


Fig. 5: Visualization of feature flow maps. The first to the fifth columns respectively list original images, corresponding feature map visualizations, optical flow from Flownet, feature flow maps from our IFF module and detection visualizations.

TABLE II: Ablation study of our IFF-Net and comparison with optical flow based methods. It shows that IFF module, TRL and Seq-NMS+ effectively improve the performance of IFF-Net.

Method	IFF module	TRL	Post-process	mAP	mAP (slow)	mAP (middle)	mAP (fast)
baseline(R-FCN)				74.1	83.6	71.6	51.2
IFF-Net-A(ours)	basic			76.0	85.0	74.8	54.7
IFF-Net-B(ours)	basic	✓		76.4	85.3	75.0	54.6
IFF-Net-C(ours)	advanced	✓		77.1	85.0	75.9	57.7
IFF-Net-D(ours)	advanced	✓	Seq-NMS	78.9	86.6	78.1	59.8
IFF-Net-E(ours)	advanced	✓	Seq-NMS+	79.7	87.5	78.7	60.6

After adding the basic IFF module, the performance (denoted as IFF-Net-A) for all categories is 76.0% mAP, 1.9% higher than our baseline. This shows that the basic IFF module improves the performance effectively. There are a 3.5% gain in mAP for fast motion category, 3.2% gain in mAP for middle motion category and 1.4% gain in mAP for slow category, respectively. After training with TRL (denoted as IFF-Net-B), the performance of the basic IFF module improves further (76.4% mAP vs 76.0% mAP). TRL not only improves the performance, but also makes the convergence faster. IFF-Net-B in Table II is the same as IFF-Net-B in Table I.

Another variant using the advanced IFF module and TRL, denoted by IFF-Net-C, is shown in the table. The mAP score increases from 76.4% to 77.1%. The performance of slow motion category is nearly unchanged after replacing basic IFF module with advance IFF module, but the mAP of fast motion category increases significantly by 3.1% (57.7 % mAP vs 54.6 % mAP). This indicates that advanced IFF module focuses on the difficult category (fast category), while yielding a similar performance on the easy category (slow category). IFF-Net-C in Table II is the same as IFF-Net-C in Table I.

Seq-NMS is widely used in existing methods, and we also explore its effectiveness in our framework. After adding Seq-NMS, the performance of our IFF-Net obtains 1.8% point gain.

This shows that Seq-NMS is also effective for our framework. By changing the Seq-NMS into Seq-NMS+ (our proposed extension of Seq-NMS), the performance improves further, with 0.8% mAP gain obtained.

D. Comparison with the state-of-the-art

Comparisons with the state-of-the-art methods are further conducted. Existing methods utilize different post-processing methods. For a fair comparison, we firstly compare IFF-Net with some methods listed in Table III without any post-processing method. All methods listed in Table III apply the same network backbone (ResNet-101). It can be seen that our IFF-Net-C (77.1% mAP) is better than FGFA [3] (76.3% mAP) and D&T [26] (75.8% mAP).

For more comprehensive comparison, we discuss other methods in Table IV, where detailed configurations for each approach is also listed. Deformable convolutional layers [39] is widely used in existing works, denoted as DCN. We also explore its effectiveness in our IFF-Net. Following DCN v1, we train our IFF-Net with 3 DCN layers (denoted as IFF-Net-F). We also investigate the number of warped images in training. Previously, we only use two neighboring images in training. In Table IV, we further evaluate our method with 4 neighboring frames warped during training. The resulting model is denoted

TABLE III: Comparison with state-of-the-art methods without any post-processing method. It shows that our IFF-Net-C achieves the best performance among other methods without post-processing method.

Method	Backbone	Post-process	mAP
IFF-Net-C(ours)	ResNet-101	No	77.1
D&T	ResNet-101	No	75.8
FGFA	ResNet-101	No	76.3

TABLE IV: Comparison with state-of-the-art methods under **different** settings. It shows that our IFF-Net-H achieves the best performance among other methods with less training dataset and smaller network on ImageNet VID validation set.

Method	Backbone	Post-process	mAP
FGFA[3]	ResNet-101 + FlowNet[9]	Seq-NMS	78.4
Zhu et al. 2017a[4]	ResNet-101(DCN) +FlowNet[9]	None	78.6
STMN[27]	ResNet-101 + DeepMask	Seq-NMS, Ensemble	80.5
D&T[26]	ResNet-101	Viterbi[37]	79.8
STSN[28]	ResNet-101(6*DCN)	Seq-NMS	80.4
PSLA [29]	ResNet-101(6*DCN)	Seq-NMS	81.4
Deng et al.[30]	ResNet-101(6*DCN)	Seq-NMS	81.6
SELSA[30]	ResNet-101(6*DCN)	Seq-NMS	80.54
RDN [38]	ResNet-101	None	81.8
IFF-Net-E(ours)	ResNet-101	Seq-NMS+	79.7
IFF-Net-F(ours)	ResNet-101(3*DCN)	Seq-NMS+	80.5
IFF-Net-G(ours)	ResNet-101(3*DCN)	Seq-NMS+	81.2
IFF-Net-H(ours)	ResNet-101(6*DCN)	Seq-NMS+	82.1



Fig. 6: Examples of detection results based on IFF-Net.

by IFF-Net-G which improves the performance of our IFF-Net (81.2% mAP). We also train a model with 6 DCN layers denoted as IFF-Net-H. Our single model, IFF-Net-H, achieves the best performance (82.1% mAP), surpassing all other methods.

Recently, some methods use ResNeXt as their backbone. Network backbone greatly influences the detection performance. For fair comparison, we only compare their performances with ResNet-101 in this paper. From Table IV, it shows that our IFF-Net-H yields the best performance among other methods. Some detection results of IFF-Net are visualized in Figure 6.

TABLE V: Time cost comparison between FlowNet and our advanced IFF module. In general, 20 neighboring frames are aggregated in video object detection. It demonstrates that our proposed IFF module is much faster than FlowNet during temporal feature aggregation.

Method	Time per Frame	Time for 20 frames
FlowNet	20 ms	400 ms
Advanced IFF module(ours)	8.8 ms	176 ms

Speed Analysis. While achieving high detection accuracy, our method is also efficient. Here we discuss the time cost of our method and compare it with other existing methods in the Table V. As our IFF-Net share a similar detection pipeline with optical flow based methods, like FGFA, we only compare time cost on the feature alignment. The time cost of FlowNet for optical flow prediction of one frame on our server is 20ms on average, which is similar to that reported in STMN. In comparison, our advanced IFF module only costs 8.8ms. As the number of warped images is 20 in optical flow based methods, time cost on FlowNet is 400ms on average. Our IFF module only costs 176ms, which is less than half of FlowNet. In summary, our framework, IFF-Net, achieves better performance than other state-of-the-art methods in the sense that it yields a fast prediction speed with less training datasets.

V. CONCLUSION

We have proposed a novel end-to-end network, IFF-Net for video object detection. Our IFF-Net is able to efficiently perform feature flow estimation for effective and efficient feature alignment. Experimental results show that our IFF-Net achieves the best result with less training datasets and a smaller network in a fast speed compared to other state-of-the-art methods.

REFERENCES

- [1] L. Chen, J. Shen, W. Wang, and B. Ni, "Video object segmentation via dense trajectories," *IEEE Transactions on Multimedia*, vol. 17, no. 12, pp. 2225–2234, 2015.
- [2] Y. Li, S. Li, C. Chen, H. Qin, and A. Hao, "Accurate and robust video saliency detection via self-paced diffusion," *IEEE Transactions on Multimedia*, 2019.
- [3] X. Zhu, Y. Wang, J. Dai, Y. Lu, and Y. Wei, "Flow-guided feature aggregation for video object detection," in *The IEEE International Conference on Computer Vision*, 2017.
- [4] X. Zhu, J. Dai, L. Yuan, and Y. Wei, "Towards high performance video object detection," in *The IEEE Conference on Computer Vision and Pattern Recognition*, 2017.
- [5] X. Zhu, Y. Xiong, J. Dai, L. Yuan, and Y. Wei, "Deep feature flow for video recognition," in *The IEEE Conference on Computer Vision and Pattern Recognition*, 2017.
- [6] Q. Peng and Y.-M. Cheung, "Automatic video object segmentation based on visual and motion saliency," *IEEE Transactions on Multimedia*, vol. 21, no. 12, pp. 3083–3094, 2019.
- [7] M. Xu, B. Liu, P. Fu, J. Li, and Y. H. Hu, "Video saliency detection via graph clustering with motion energy and spatiotemporal objectness," *IEEE Transactions on Multimedia*, vol. 21, no. 11, pp. 2790–2805, 2019.
- [8] J.-Y. Liu, Y.-H. Yang, and S.-K. Jeng, "Weakly-supervised visual instrument-playing action detection in videos," *IEEE Transactions on Multimedia*, vol. 21, no. 4, pp. 887–901, 2018.
- [9] A. Dosovitskiy, P. Fischer, E. Ilg, P. Hausser, C. Hazirbas, V. Golkov, P. Van Der Smagt, D. Cremers, and T. Brox, "Flownet: Learning optical flow with convolutional networks," in *The IEEE International Conference on Computer Vision*, 2015.
- [10] W. Han, P. Khorrami, T. L. Paine, P. Ramachandran, M. Babaeizadeh, H. Shi, J. Li, S. Yan, and T. S. Huang, "Seq-nms for video object detection," *arXiv preprint arXiv:1602.08465*, 2016.
- [11] O. Russakovsky, J. Deng, H. Su, J. Krause, S. Satheesh, S. Ma, Z. Huang, A. Karpathy, A. Khosla, M. Bernstein, *et al.*, "Imagenet large scale visual recognition challenge," *International Journal of Computer Vision*, 2015.
- [12] R. Girshick, J. Donahue, T. Darrell, and J. Malik, "Rich feature hierarchies for accurate object detection and semantic segmentation," in *The IEEE Conference on Computer Vision and Pattern Recognition*, 2014.
- [13] R. Girshick, "Fast r-cnn," in *The IEEE International Conference on Computer Vision*, 2015.
- [14] S. Ren, K. He, R. Girshick, and J. Sun, "Faster r-cnn: Towards real-time object detection with region proposal networks," in *Advances in Neural Information Processing Systems*, 2015.
- [15] J. Dai, Y. Li, K. He, and J. Sun, "R-fcn: Object detection via region-based fully convolutional networks," in *Advances in Neural Information Processing Systems*, 2016.
- [16] T.-Y. Lin, P. Dollár, R. B. Girshick, K. He, B. Hariharan, and S. J. Belongie, "Feature pyramid networks for object detection," in *The IEEE Conference on Computer Vision and Pattern Recognition*, 2017.
- [17] A. Shrivastava, R. Sukthankar, J. Malik, and A. Gupta, "Beyond skip connections: Top-down modulation for object detection," *arXiv preprint arXiv:1612.06851*, 2016.
- [18] P. Sermanet, D. Eigen, X. Zhang, M. Mathieu, R. Fergus, and Y. LeCun, "Overfeat: Integrated recognition, localization and detection using convolutional networks," in *International Conference on Learning Representations*, 2014.
- [19] J. Redmon, S. Divvala, R. Girshick, and A. Farhadi, "You only look once: Unified, real-time object detection," in *The IEEE Conference on Computer Vision and Pattern Recognition*, 2016.
- [20] J. Redmon and A. Farhadi, "Yolo9000: better, faster, stronger," *The IEEE Conference on Computer Vision and Pattern Recognition*, 2017.
- [21] W. Liu, D. Anguelov, D. Erhan, C. Szegedy, S. Reed, C.-Y. Fu, and A. C. Berg, "Ssd: Single shot multibox detector," in *European Conference on Computer Vision*, 2016.
- [22] T.-Y. Lin, P. Goyal, R. Girshick, K. He, and P. Dollár, "Focal loss for dense object detection," *The IEEE International Conference on Computer Vision*, 2017.
- [23] M. Everingham, L. Van Gool, C. K. Williams, J. Winn, and A. Zisserman, "The pascal visual object classes (voc) challenge," *International journal of computer vision*, 2010.
- [24] K. Kang, H. Li, J. Yan, X. Zeng, B. Yang, T. Xiao, C. Zhang, Z. Wang, R. Wang, X. Wang, *et al.*, "T-cnn: Tubelets with convolutional neural networks for object detection from videos," *IEEE Transactions on Circuits and Systems for Video Technology*, 2017.
- [25] K. Kang, W. Ouyang, H. Li, and X. Wang, "Object detection from video tubelets with convolutional neural networks," in *The IEEE Conference on Computer Vision and Pattern Recognition*, 2016.
- [26] C. Feichtenhofer, A. Pinz, and A. Zisserman, "Detect to track and track to detect," in *The IEEE Conference on Computer Vision and Pattern Recognition*, 2017.
- [27] F. Xiao and Y. J. Lee, "Video object detection with an aligned spatial-temporal memory," in *European Conference on Computer Vision*, 2018.
- [28] G. Bertasius, L. Torresani, and J. Shi, "Object detection in video with spatiotemporal sampling networks," in *Proceedings of the European Conference on Computer Vision (ECCV)*, pp. 331–346, 2018.

- [29] C. Guo, B. Fan, J. Gu, Q. Zhang, S. Xiang, V. Prinet, and C. Pan, "Progressive sparse local attention for video object detection," *ICCV*, 2019.
- [30] H. Deng, Y. Hua, T. Song, Z. Zhang, Z. Xue, R. Ma, N. Robertson, and H. Guan, "Object guided external memory network for video object detection," in *Proceedings of the IEEE International Conference on Computer Vision*, pp. 6678–6687, 2019.
- [31] H. Wu, Y. Chen, N. Wang, and Z. Zhang, "Sequence level semantics aggregation for video object detection," in *Proceedings of the IEEE International Conference on Computer Vision*, pp. 9217–9225, 2019.
- [32] M. Shvets, W. Liu, and A. C. Berg, "Leveraging long-range temporal relationships between proposals for video object detection," in *Proceedings of the IEEE International Conference on Computer Vision*, pp. 9756–9764, 2019.
- [33] K. Kang, H. Li, T. Xiao, W. Ouyang, J. Yan, X. Liu, and X. Wang, "Object detection in videos with tubelet proposal networks," in *The IEEE Conference on Computer Vision and Pattern Recognition*, 2017.
- [34] K. Chen, J. Wang, S. Yang, X. Zhang, Y. Xiong, C. Change Loy, and D. Lin, "Optimizing video object detection via a scale-time lattice," in *Proceedings of the IEEE conference on computer vision and pattern recognition*, pp. 7814–7823, 2018.
- [35] K. He, X. Zhang, S. Ren, and J. Sun, "Deep residual learning for image recognition," in *The IEEE Conference on Computer Vision and Pattern Recognition*, 2016.
- [36] C. Zach, T. Pock, and H. Bischof, "A duality based approach for realtime tv-l 1 optical flow," in *Joint Pattern Recognition Symposium*, 2007.
- [37] G. Gkioxari and J. Malik, "Finding action tubes," in *The IEEE Conference on Computer Vision and Pattern Recognition*, 2015.
- [38] J. Deng, Y. Pan, T. Yao, W. Zhou, H. Li, and T. Mei, "Relation distillation networks for video object detection," in *Proceedings of the IEEE International Conference on Computer Vision*, pp. 7023–7032, 2019.
- [39] J. Dai, H. Qi, Y. Xiong, Y. Li, G. Zhang, H. Hu, and Y. Wei, "Deformable convolutional networks," in *The IEEE International Conference on Computer Vision*, 2017.